Advances in Geo-Energy Research

Vol. 15, No. 3, p. 261-272, 2025

Original article

Expansion-induced fracture propagation in deep geothermal reservoirs under alternate-temperature loading

Daobing Wang[1], Yongcun Dong[1], Chunlei Wei[1], Qitao Zhang[2], Mao Sheng[3], Bo Yu[4]

[1]*School of Mechanical Engineering, Beijing Institute of Petrochemical Technology, Beijing 102617, P. R. China*

[2]*Department of Energy and Mineral Engineering, The Pennsylvania State University, University Park, PA 16802, USA*

[3]*School of Petroleum Engineering, China University of Petroleum (Beijing), Beijing 102249, P. R. China*

[4]*School of Petroleum Engineering, Yangtze University, Wuhan 430100, P. R. China*

Keywords:
Deep geothermal reservoir
alternate-temperature loading
rock mechanics
artificial fracture network
expansion fracturing

Cited as:
Wang, D., Dong, Y., Wei, C., Zhang, Q., Sheng, M., Yu, B. Expansion-induced fracture propagation in deep geothermal reservoirs under alternate-temperature loading. Advances in Geo-Energy Research, 2025, 15(3): 261-272.
https://doi.org/10.46690/ager.2025.03.08

Abstract:
Hydraulic fracturing is a crucial technique for the extraction of geothermal energy from hot dry rock reservoirs. However, the development of such reservoirs faces significant challenges due to the high *in-situ* stress and strong elastic-plastic behavior of these rocks, which often result in simplified fracture geometries and subsequent low heat extraction efficiency. To address this issue, a novel reservoir treatment method based on thermal expansion and contraction principles is proposed. By applying alternating heating-cooling treatments to the reservoir, cyclic thermal stress is generated within the rock to enhance the complexity of post-fracturing fracture networks. To investigate the resultant hydraulic fracture propagation under alternate-temperature loading, a custom-developed thick-walled cylinder expansion fracturing device was employed to study the fracture propagation mechanisms in hot dry rock samples under cyclic thermal loading. The fracture network complexity was characterized by the fractal dimension method. Experimental results demonstrated that alternate thermal load cycling significantly enhances the fracture network complexity compared to conventional single-phase heat treatment. The maximum improvement in fractal dimension (3.86% increase) was observed at 500 °C. Under alternating temperature loads, the upper surface fractures predominantly exhibited bilateral symmetric structures. At 600 °C, a substantial increase in branched fractures and rock debris near boreholes occurred, indicating that alternating temperature loads significantly enhance the complexity of engineered fracture networks in hot dry rock. These findings suggest that incorporating thermal cycling into hydraulic fracturing processes can significantly improve the fracture network complexity, thereby enhancing the efficiency of heat extraction from hot dry rock reservoirs.

1. Introduction

Hydraulic fracturing is increasingly used to improve heat extraction from deep thermal reservoirs (Kumari et al., 2018; Moska et al., 2024). The process involves injecting fracturing fluid at a pressure exceeding the reservoir's breakdown pressure to create seepage channels, enhancing heat extraction from hot dry rock (HDR) (Cheng et al., 2020; Moska et al., 2021). However, HDR reservoirs are often characterized by deep burial, high *in-situ* stress anisotropy and elastoplastic deformation, leading to simpler fracture networks. During water injection, this can cause fluid short-circuiting and "thermal breakthrough," reducing the heat extraction efficiency (Wang et al., 2023b; Liu et al., 2024). Therefore, understanding fracture propagation and increasing fracture complexity are

Yandy Scientific Press

*Corresponding author.
E-mail address: upcwdb@bipt.edu.cn (D. Wang); dongyc_bipt@163.com (Y. Dong); 2023520143@bipt.edu.cn (C. Wei); qpz5080@psu.edu (Q. Zhang); shengmao@cup.edu.cn (M. Sheng); yubobox@vip.163.com (B. Yu).

Received January 5, 2025; revised February 1, 2025; accepted February 25, 2025; available online March 2, 2025.

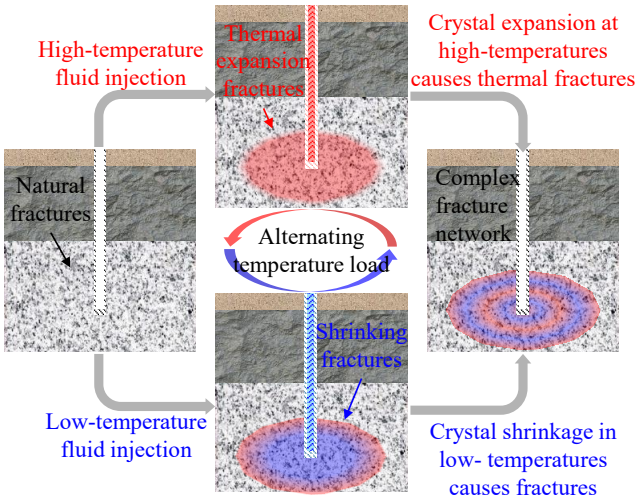

Fig. 1. Schematic diagram of alternating temperature load principle.

critical for improving HDR heat extraction.

The current research in this field mainly relies on numerical simulations and laboratory experiments (Cheng et al., 2021; Wang et al., 2024c). Researchers have studied the influence of various factors on fracture propagation, like natural fractures, *in-situ* stress, fracturing fluid viscosity, injection rate, and reservoir temperature (Cheng et al., 2021; Luo and Liu, 2022). Discrete fracture network modeling has shown that pre-existing fractures modulate fracture trajectories, promoting complex network development (Li, 2020; Li et al., 2021). However, excessive natural fractures can limit fracture propagation due to energy dissipation (Wang et al., 2024c). Advanced thermo-hydro-mechanical-damage coupling models have highlighted the effects of stress anisotropy on fracture behavior, with fractures aligning with the maximum horizontal principal stress (Guo et al., 2020). The fracture complexity is influenced by the injection rate and fluid dynamics, with higher rates fostering secondary branching (Cheng et al., 2021). As for viscosity, it affects fracture propagation, with low-viscosity fluids promoting microfractures, while high-viscosity fluids hindering extension (Ma et al., 2022). Thermal effects also influence fracture propagation, with high temperatures reducing fracture initiation pressure and enhancing branching (Xue et al., 2023).

Despite the benefits of numerical simulations, assumptions and simplifications can lead to errors, making laboratory experiments essential for understanding fracture propagation mechanisms. Experimental studies have identified key factors like *in-situ* stress anisotropy, natural fractures and rock mass damage state. Kao et al. (2018) found a correlation between horizontal stress differential and fracture initiation pressure, with higher stress contrasts requiring higher breakdown pressures. Hydraulic fractures propagate along the maximum principal stress direction under high stress differences, aligning with the classical fracture mechanics theory (Wang, 2019; Zheng et al., 2022). Injection rate and thermal stress also affect fracture initiation pressure and propagation: higher injection rates lead to higher breakdown pressures and more complex fracture networks (Hou et al., 2014). Thermal treatment experiments have shown that elevated temperatures reduce the mechanical properties of granite, enhancing fracture formation (Wang et al., 2023a; Li et al., 2024; Wang et al., 2024a). Thermal stress also reduces breakdown pressure, facilitating more complex fracture networks (Luo and Liu, 2022; Xue et al., 2023; Wang et al., 2024b).

Thermal cycling, which involves alternating hot and cold fluid injections, simulates thermal stresses in subsurface reservoirs (Yang et al., 2024), which in turn induce expansion and contraction within the rock, leading to stress fields that enhance fracture complexity (Fig. 1). These combined effects improve heat extraction in enhanced geothermal systems (EGS) and unconventional hydrocarbon reservoirs (Wang et al., 2022). Therefore, understanding fracture propagation under thermal stress is crucial for the improvement of heat extraction efficiency.

Fractal dimension, as a nonlinear geometric parameter, provides an effective means of characterizing the spatial heterogeneity and morphological complexity of rock fracture networks, rendering it a valuable tool for analyzing microfracture propagation induced by thermal cycling (Barton, 1995). Unlike traditional computed tomography (CT) scanning, which requires high-precision equipment and complex three-dimension (3D) reconstruction, fractal dimension offers an inexpensive and efficient alternative for fracture network characterization. It allows for the quantification of fracture branching density, connectivity and self-similarity through two dimensions or 3D image processing, addressing the scalability and cost challenges associated with CT scanning (Zhuang et al., 2022; Yu et al., 2024).

Through thermal maturity experiments on oil shale at temperatures ranging from 200-600 °C, microstructural images were analyzed to extract fracture fractal dimensions (ranging from 1.0 to 1.5). This enabled the quantification of microfluidic pathway evolution during pyrolysis. Similarly, uniaxial compression tests on rock-like materials demonstrated that fractal dimension is closely related to key mechanical parameters, such as fracture initiation stress and peak strain, providing a basis for predicting the expansion of dynamic fracture networks. Furthermore, fractal algorithms based on morphological theory and computer image processing, including the box-counting method and the δ-right triangle area-covering method, have been widely applied in edge extraction and fractal dimension calculations for soil fissures and rock surface fractures. These applications underscore the versatility of these methods in petroleum and geothermal engineering (Mandelbrot, 1967; Guo et al., 2013; Zhuang et al., 2022).

Fractal dimension serves as a powerful tool for quantifying the self-similarity of complex fracture networks, offering critical insights into fracture propagation under conditions of thermal stress. Previous studies have established a strong correlation between fractal dimension and fundamental fracture parameters such as initial aperture and tortuosity (Cai et al., 2017; Sheng et al., 2019). For instance, a higher fractal dimension of the aperture has been associated with weaker slip effects and reduced permeability sensitivity to pressure variations. Additionally, three-dimensional fractal vector models showed that variations in fractal dimension across different

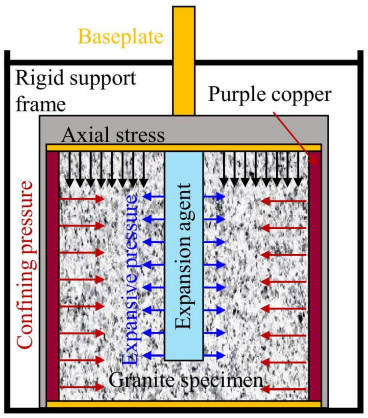

Fig. 2. Thick-walled cylinder device for expansion fracturing and rock samples.

directions (anisotropy) directly affect the material properties, such as compressive strength and permeability distribution (Zhang et al., 2023).

Under thermal cycling, fractal dimension captures the impact of temperature gradients on fracture distribution. Higher temperatures result in increased fractal dimension values, indicating the development of denser microfracture networks (Pan et al., 2024). The fractal interpolation theory further enables the construction of spatial fractal curves, effectively modeling the three-dimensional propagation of fractures within a thermal stress field. Unlike static imaging techniques such as CT scanning, this fractal-based approach is particularly suited for analyzing the progressive accumulation of thermal damage caused by cyclic thermal stress (Deng et al., 2023). Moreover, it offers theoretical guidance for optimizing thermal-hydraulic cycling parameters, such as temperature differentials and injection frequency, which is crucial for both geothermal energy extraction and hydraulic fracturing optimization.

Traditional studies on fracture propagation have mainly focused on factors like injection rate, *in-situ* stress fields, and single-temperature variations. However, research on the formation mechanisms of artificial fracture networks under alternating thermal loads from hydraulic fracturing remains limited. To enhance fracture complexity and improve heat extraction efficiency in deep geothermal reservoirs, this study investigated the effects of thermal expansion and contraction. Rock samples were subjected to alternating thermal treatments, where they were first heated and then rapidly cooled using liquid nitrogen. This process amplifies the thermal stress within the rock, leading to the formation of complex artificial fractures. The resulting fracture complexity was quantitatively assessed through fractal dimension analysis.

This study introduces innovative methods, including alternating thermal loading (heating followed by rapid cooling) and fractal dimension analysis (using the box-counting method), to explore the fracture network evolution under thermal stress. By simulating more realistic subsurface conditions, alternating thermal loading induces significant thermal stresses that enhance fracture complexity. Fractal dimension analysis allows for a detailed assessment of fracture irregularities across multiple scales, providing deeper insights into how thermal stresses influence the fracture morphology. Fractures formed under thermal cycling were compared with those created by simple heating, which reveals how thermal cycles lead to more intricate and heterogeneous fracture networks. This comparative approach highlights the importance of thermal stress cycles in creating complex fracture patterns, which are essential for improving heat extraction efficiency in geothermal and unconventional hydrocarbon systems. The findings of this work advance the optimization of fracturing strategies and geothermal energy extraction.

2. Experimental materials and device

2.1 Rock samples

The rock samples utilized for this experiment were extracted from granite outcrops in Mi'luo, Hunan Province, South China. The core was processed into cylindrical specimens with a diameter of 107.5 mm and a height of 130 mm. The outer surface of each core was polished, and a circular hole with a diameter of 16 mm and a depth of 130 mm was drilled at the center of each rock sample.

2.2 Laboratory setup

In order to simulate the expansion mechanism of artificial fracture networks under expansion fracturing in high-permeability core formations while considering the *in-situ* stress characteristics of deep geothermal reservoirs, this study independently designed an experimental device for the expansion fracturing of thick-walled cylinders in high-permeability cores. This device has been granted a Chinese invention patent (Dong et al., 2021). The experimental apparatus consists of three main structural components: a precision-engineered core confinement assembly, a rigid main support frame, and adjustable baseplate limiting rods. The cylindrical rock core specimen is precisely positioned within the confinement assembly, where calibrated horizontal stress is applied by inserting copper shims or thin-gauge steel plates into the annular space. As shown in Fig. 2, upon the injection of chemically reactive expansive agents into the core matrix, controlled axial stress is progressively applied through the torque-regulated downward displacement of the baseplate limiting rods. This integrated mechanical system replicates the triaxial stress conditions encountered in subsurface formations, enabling the precise simulation of fracture network development resulting from expansive fracturing mechanisms under representative confining pressure environments (Guo et al., 2013). Considering the material properties of the annular thick-walled cylinder and the optimal fracture initiation size for expansion fracturing, the inner diameter and wall thickness of the expansion fracturing thick-walled cylinder device were designed to be 108 and 8 mm, respectively.

2.3 Experimental procedure

Twelve sample groups consisting of 24 homogeneous granite cores (2 cores per group) were subjected to controlled thermal treatment. The temperature protocol involved heating from ambient temperature to target temperatures of 100, 200,

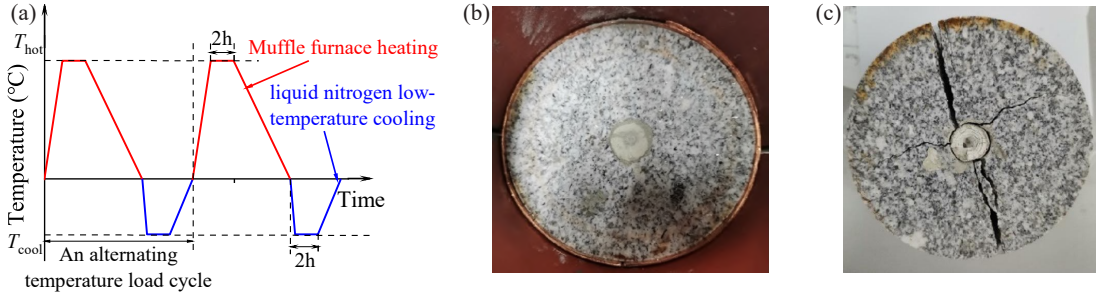

Fig. 3. Experimental process of expansion fracturing: (a) Alternating temperature load treatment of rock samples, (b) injection of expansion agent and (c) fracture morphology.

300, 400, 500, and 600 °C at a controlled rate of 5 °C/min, followed by a 2-hour isothermal holding period at each target temperature value. Afterwards, the samples were cooled to room temperature at the same rate. The thermal shock cycle was completed by immersing the samples in liquid nitrogen for 2 hours, as shown in Fig. 3.

In order to evaluate the development of fracture networks in HDR under alternating thermal conditions, a comparative analysis was conducted between samples subjected to alternating temperature loads and those treated with conventional heating alone. The comparison focused on the morphological characteristics of the artificial fracture networks, specifically their expansion patterns and structural complexity under different thermal treatment regimes.

Experimental studies in rock fracture mechanics have emphasized the critical role of controlled stress conditions in creating representative fracture networks. The thick-walled cylinder testing apparatus has significantly improved the simulation accuracy of *in-situ* stress conditions during rock fracturing processes. Therefore, as shown in Fig. 3, the samples to be tested were selected and placed into the thick-walled cylinder. Copper sheet gaskets were inserted into the gaps between the samples and the cylinder, and the screws on the cylinder were tightened. The expanding agent was prepared according to the specified proportions and quickly injected into the boreholes. Vertical stress was applied, and the samples were placed in a cool environment and left to stand for over 48 hours for expansion fracturing. Subsequently, the samples were removed and the complexity of fractures was analyzed using the fractal dimension.

3. Fractal theory and methods

3.1 Fractal dimension

In order to quantitatively describe the complexity of fractures generated by expansion fracturing, fractal dimension was employed: The fractal dimension of fracture surfaces was calculated using the box-counting method. Based on the definition of fractal dimension, the distribution of fractures across different scales follows the equation below (Mandelbrot, 1967):

$$N(\delta) = A\delta^{-D} \tag{1}$$

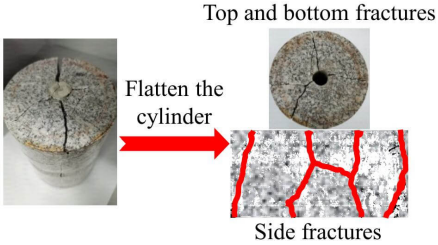

Fig. 4. Expanded view of the outer surface of rock samples.

where δ represents the side length, N represents the number of fractures, A is the initial value of the fracture surface distribution that is equal to the number of fractures with an area greater than δ^2 in the rock, and D denotes the fractal dimension of the fracture distribution. The following formula was derived by taking the logarithm of both sides of Eq. (1):

$$\lg N(\delta) = \lg A - D\lg\delta \tag{2}$$

Since the actual fracture morphology is three-dimensional, an accurate determination of the fractal dimension requires unfolding the cylinder into its top, bottom and side surfaces, as illustrated in Fig. 4. On the basis of cylindrical geometry principles, the fractal dimensions of these three surfaces were calculated individually, then their arithmetic mean was computed to obtain the final fractal dimension. The specific steps were as follows: First, a high-precision camera was used to capture images of the fracture morphologies on the top and bottom surfaces. For the fracture morphology on the side surface, a piece of white paper of the same size was wrapped around the outer surface. Using the unevenness of the outer surface and the fracture directions as a guide, the fracture patterns on the paper were marked with a marker pen.

3.2 Calculation method

Rock mechanics utilize fractal analysis to evaluate multi-scale damage in underground reservoirs. The grid-based fractal method effectively analyzes fracture networks across various scales, proving particularly useful for assessing geothermal reservoir complexity. Modern computational techniques employ multi-scale grids to study heat-induced fracture patterns, surpassing traditional methods in the analysis of complex rock formations. As shown in Fig. 5, the areas divided by the red, green and blue straight lines represent covering grids of different sizes. The maximum grid size was set as half the di-

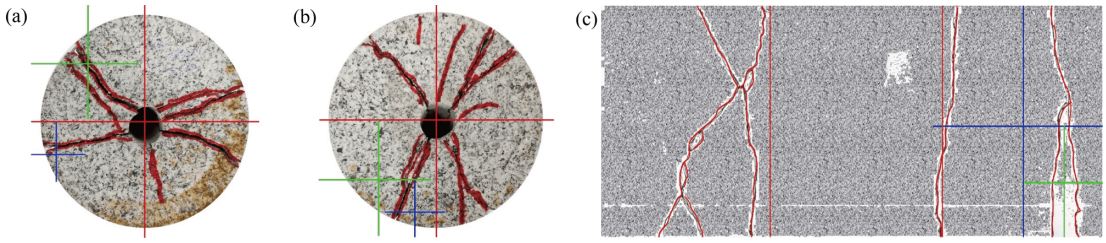

Fig. 5. Fracture morphology in (a) upper bottom view, (b) lower bottom view and (c) side view.

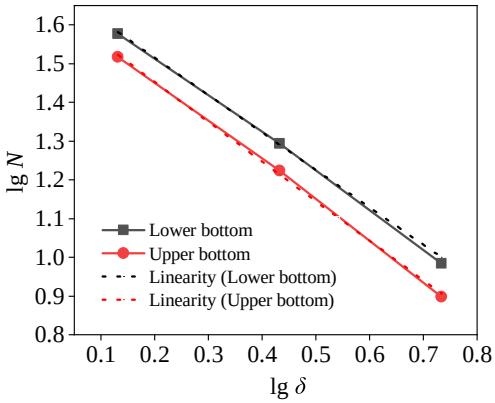

Fig. 6. Calculation of fractal dimension of the upper and lower underside.

ameter of the rock sample. By varying the grid size, the number of fractures within each corresponding grid could be counted. As shown in Fig. 6, the logarithm of the fracture side length was taken as the independent variable, and that of the number of fractures was taken as the dependent variable. The least squares method was then used to perform linear fitting on the curve in a double logarithmic coordinate system. The fractal dimension of the fractures on that surface is given by the absolute value of the slope of the resulting curve.

4. Experimental results

4.1 Variation of fractal dimension

The fractal dimensions of the fracture networks generated by the expansion fracturing of HDR, both after simple heat treatment and under alternating temperature loads, were calculated using the fractal dimension, as shown in Fig. 7. The comprehensive analysis of experimental results demonstrated that thermal cycling through alternating temperature loads significantly enhances fracture network complexity compared to conventional monotonic heating treatments. Quantitative evaluation using fractal dimension analysis revealed a progressive increase in network complexity with rising temperature, with the optimal enhancement achieved at 600 °C thermal cycling conditions. This temperature-dependent behavior indicated that cyclic thermal loading induces more effective stress redistribution and fracture branching mechanisms in HDR compared to static thermal treatments. The observed fractal dimension trends confirmed that controlled thermal cycling represents a promising approach for optimizing fracture network complexity in HDR reservoirs, potentially leading to improved heat exchange efficiency in EGS.

Temperature changes significantly affect fracture patterns in brittle materials. Fractal analysis effectively measures fracture network complexity under different thermal conditions. Studies have shown that thermal stress and material changes control fracture shapes, with fractal dimension serving as a key damage indicator. The results shown in Fig. 7(a) illustrate the variation trend of the fractal dimensions of expansion fracturing on the upper and bottom surfaces after simple heat treatment and under alternating temperature loads. As the temperature rises, the fractal dimension of expansion fracturing under alternating temperature loads exhibits a linear upward trend, with an increase of 9.6% from 100 to 600 °C. The growth rate of the fractal dimension of expansion fracturing after heat treatment is relatively slow from 100 to 500 °C, with an increase of only 0.034%. However, from 500 to 600 °C, the growth rate accelerates, reaching 6.3%. Compared to simple heat treatment, the fractal dimension of expansion fracturing under alternating temperature loads shows a significant growth. As the temperature rises, the range of increase in fractal dimension first enlarges and then decreases, with the maximum increase of 7.4% occurring at 500 °C.

Thermal fracturing mechanisms exhibit distinct differences in fracture network development across varying thermal histories. The evolution of fracture complexity with temperature offers crucial insights into reservoir stimulation effectiveness. Fig. 7(b) presents the variation in the fractal dimension of expansion fracturing on the lower bottom surface of the sample. It can be seen that the fractal dimension of expansion fracturing in HDR subjected to alternating temperature loads is consistently higher than that observed after simple heat treatment. Notably, the fractal dimension under alternating temperature loads exhibits a decreasing trend between 100 and 200 °C. However, beyond 200 °C, it increases at a significantly higher rate, with a marked 13.8% rise from 500 to 600 °C. In contrast, the fractal dimension after simple heat treatment remains relatively stable from 100 to 400 °C, with only a marginal increase. From 400 to 600 °C, this value experiences a maximum increase of 15.3%. A comparative analysis of the fractal dimension changes under the two treatment methods revealed that at 200 °C, the fractal dimension under alternating temperature loads is lower than that after simple heat treatment, which is potentially attributable to variations in core homogeneity. Importantly, at 600 °C, the fractal dimension under alternating temperature loads shows a maximum increase of 7.8% compared to that after simple heat treatment.

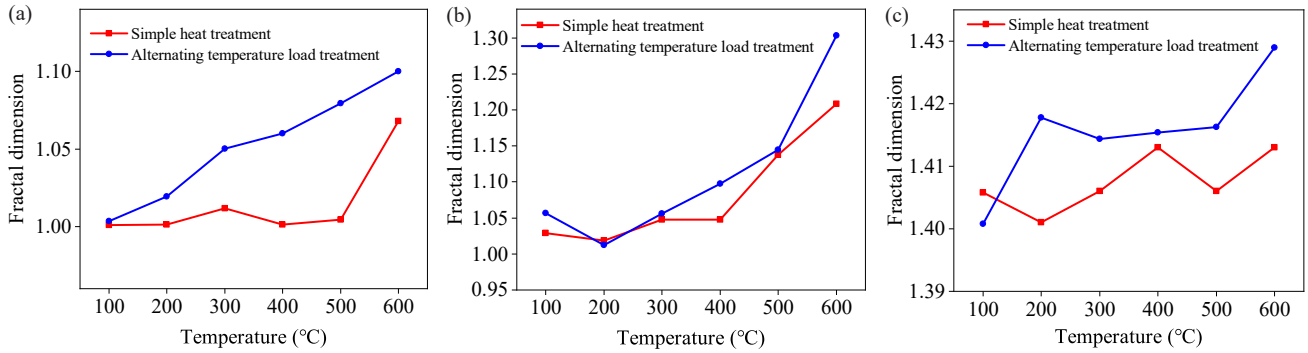

Fig. 7. Fractal dimension of each surface fracture after expansion fracturing under alternating temperature loading: (a) Upper bottom view, (b) lower bottom view and (c) side view.

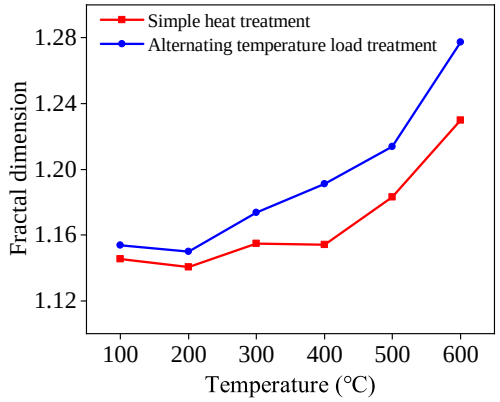

Fig. 8. Fractal dimension of HDR after expansion fracturing under alternating temperature loads.

Thermal fracture analysis reveals significant differences in fracture growth between cyclic and steady heating conditions. In geothermal engineering, understanding fracture network responses to temperature variations is essential. Repeated heating and cooling generate unique fracture patterns through stress reversal, altering energy release mechanisms compared to constant heating. Fig. 7(c) presents the variation curve of fracture fractal dimension on the sample's side surface after expansion fracturing. The analysis shows distinct patterns in fractal dimension evolution under different thermal conditions. Under alternating temperature loads, the fractal dimension demonstrates a non-monotonic trend, characterized by an initial increase followed by a decrease and subsequent rise. In contrast, samples subjected to simple heat treatment exhibit a different multi-stage pattern, showing an initial decrease followed by an increase, while maintaining an overall upward trend with the temperature increasing. Notably, the fractal dimension changes under both thermal conditions lack a clear, consistent correlation with temperature elevation.

A comparison of the fractal dimensions of expansion fracturing under the two heat treatment methods indicates that the fractal dimension after alternating temperature loads is significantly higher than that after simple heat treatment. This suggests that alternating temperature loads reduce the mechanical strength of HDR, thereby enhancing the complexity of the artificial fracture network generated by expansion fracturing.

Understanding the full complexity of thermal-induced fracture networks requires moving beyond surface-specific analysis and performing system-level characterization. To this end, the integration of multi-surface fractal data provides critical insights into the three-dimensional evolution of fracture networks under thermal cycling. Fig. 7 illustrates the fractal dimension distributions of expansion-induced fractures on the upper, lower and side surfaces of the experimental rock samples. The preceding analysis individually examined the impact of thermal cycling on the fractal characteristics of each specific surface. Although this segmented approach provides valuable insights into localized fracture patterns, it necessitates a more systematic investigation to elucidate the comprehensive thermal response of fracture networks in HDR under cyclic thermal loading. A robust evaluation of the thermal effects on fracture network complexity requires an integrated analysis of all external surfaces, which enables the characterization of system-level fractal behavior in expansion-induced fracture systems under alternating temperature conditions.

New methods in damage analysis highlight the utility of 3D fractal characterization in assessing geothermal reservoir effectiveness. Furthermore combining surface fracture data helps measure heat-induced damage, especially for improving directional flow. Research has shown that repeated heating creates unique fracture networks by connecting old and new fractures, forming better flow paths than standard heating methods. As illustrated in Fig. 8, the fractal dimensions of the upper and lower bottom surfaces and the side surface of the sample were summed and averaged to determine the overall fractal dimension of the sample. It is clearly demonstrated in the figure that the fractal dimension of expansion fracturing in HDR subjected to alternating temperature loads is significantly higher than that after simple heat treatment. This finding strongly indicates that alternating temperature loads play a crucial role in enhancing the complexity of the fracture network generated by expansion fracturing in HDR. Furthermore, the fractal dimension under alternating temperature loads increases with rising temperature. At 600 °C, the maximum fractal dimension reaches 1.28, representing an increase of 3.86% compared to the value observed after simple heat treatment.

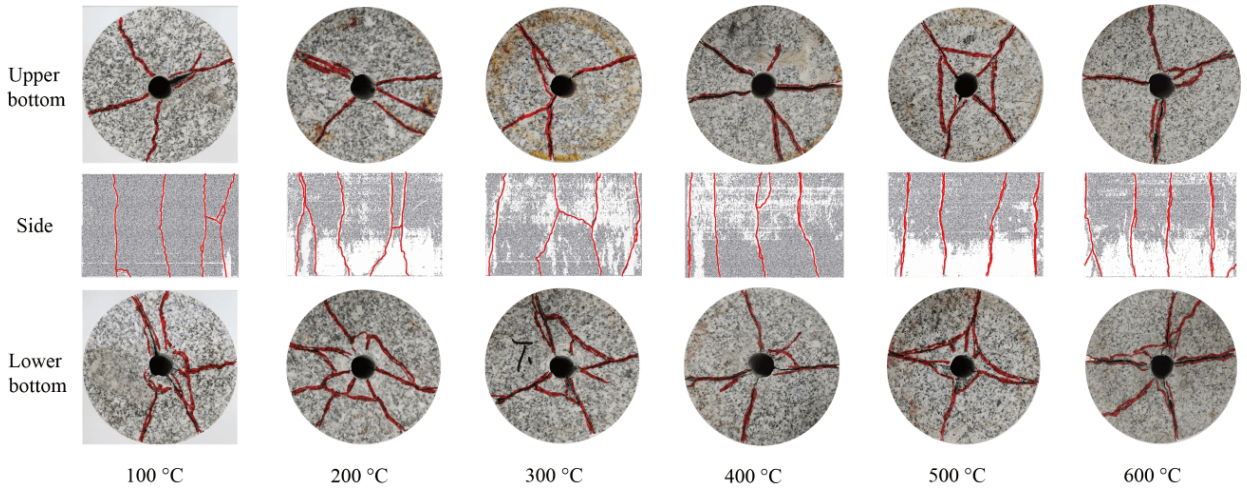

Fig. 9. Fracture network morphology caused by expansion fracturing of hot dry rock after heat treatments: Fracture morphology of expansion fracturing after heat treatment at 100, 200, 300, 400, 500, and 600 °C.

4.2 Variations in fracture number and morphology

Studies on rock fractures have indicated that surface fracture patterns are key to evaluating reservoir stimulation. Digital imaging has shown that heat-induced fractures depend on temperature changes, stress conditions and rock properties. In geothermal systems, differences in fracture patterns between surfaces indicate reservoir anisotropy, with lower surfaces often exhibiting hidden damage from heat and gravity. In Fig. 9, the morphologies of fracture networks affected by expansion fracturing on the upper and lower bottom surfaces and the side surface of HDR after simple heat treatment are presented, where the red line markers indicate the fracture propagation paths. From the upper and lower bottom surfaces, it can be observed that the fractures primarily extend from the prefabricated boreholes to the surface edges. On the upper bottom surface, 3 to 4 main fractures are present, while on the lower bottom surface, 4 to 5 main fractures can be found. Due to the circumferential stress constraints around the rock samples, the main fractures are symmetrically distributed in a double-wing pattern. Additionally, a significant number of fragments fall off near the boreholes, with the quantity of fragments increasing as the temperature rises. Under this condition, multiple branch fractures form near the main fractures, interconnecting with them and thus contributing to a more complex fracture network structure. Fig. 9 clearly shows that the number and complexity of fractures on the lower bottom surface are significantly greater than those on the upper bottom surface.

After the expansion fracturing of rock samples, the side fractures appear to be distributed in parallel, with nearly equal spacing between each fracture. Each sample has four main fractures that extend through both the upper and lower bottom surfaces. The degree of curvature and complexity of each fracture gradually increases with the temperature rising. Above 300 °C, under the action of expansion forces, branch fractures extend from the main fractures in the rock samples treated at different temperatures. This indicates that with increasing temperature, the complexity of the fracture network created by the expansion fracturing of HDR becomes significantly enhanced.

Research on repeated heating and cooling has identified the key principles controlling fracture patterns. Thermal mapping has demonstrated that temperature variations create distinct fracture paths via combined hardening and weakening effects, particularly in crystalline rocks. Geothermal studies reported that cyclic thermal loading generates organized fracture networks that enhance fluid flow while preserving rock integrity, with secondary fractures significantly improving permeability. Fig. 10 shows the fracture network morphology caused by the expansion and fracture of HDR under the action of alternating temperature loads. It can be seen that the number and complexity of artificial fractures on the lower surface of granite after expansion fracture are greater than those on the upper surface. In addition to the fractures expanding around the wellbore, multiple branch fractures also develop from the main fracture propagation. When the temperature of the alternating temperature loads is between 100 and 200 °C, three main fractures form on the upper bottom surface, with the angles between adjacent fractures being approximately 120°. As the temperature reaches 300 °C, the fractures on the upper bottom surface gradually adopt a double-wing symmetrical distribution. The angle between the two fractures in each wing initially decreases and then increases with rising temperature. Additionally, a branch fracture forms perpendicular to the double-wing fractures, further enhancing the complexity of fractures after expansion fracturing.

After treatment with alternating temperature loads, the fracture network on the lower bottom surface becomes more intricate. When the temperature is between 100 and 200 °C, multiple small fractures develop near the main fractures due to expansion. As the temperature exceeds 300 °C, the thermal shock effect induced by the alternating temperature loads intensifies. According to rock mechanics experiments, higher temperature lowers the mechanical strength of the rock after

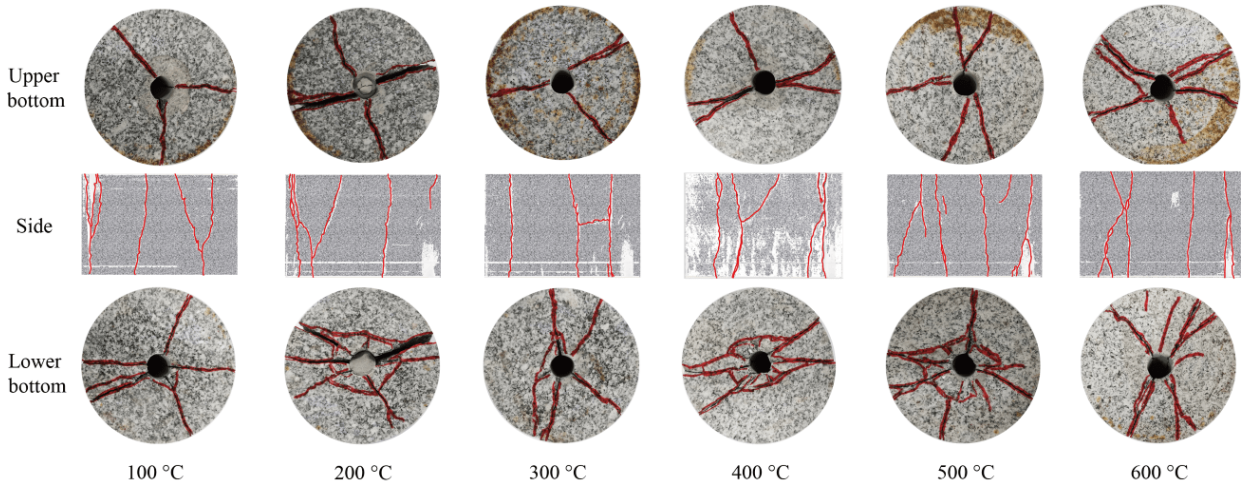

Fig. 10. Fracture network morphology caused by the expansion fracturing of hot dry rocks after alternating temperature loading: The expansion fracture morphology after alternating temperature loading at 100, 200, 300, 400, 500 and 600 °C.

alternating temperature load treatment. Consequently, after expansion fracturing on the lower bottom surface, numerous microfractures extend from the vicinity of the wellbore. As these microfractures gradually connect and form macroscopic fractures, the main fractures interconnect, ultimately resulting in a complex fracture structure.

After the rock samples have undergone alternating temperature loads and expansion fracturing, the fractures on the side surfaces exhibit varying spacing sizes, with their geometric distribution appearing complex and disordered. Between 3 and 4 main fractures extend through the upper and lower bottom surfaces of the rock samples. Multiple branching fractures continue to form from different positions along the main fractures. Some of these fractures extend to the upper and lower bottom surfaces, while others interconnect several main fractures horizontally. As the heating temperature rises, particularly in the range of 400 to 500 °C, the thermal and cold shock effects from alternating temperature loads result in multiple fractures appearing on the side surfaces of the rock samples after expansion fracturing, along with numerous microfractures distributed on the surfaces. This observation confirms that the complexity of the fracture network caused by the expansion fracturing of HDR under alternating temperature loads is significantly greater than that observed after simple heat treatment.

When comparing the fracture network structures of HDR caused by expansion fracturing between after simple heat treatment and after alternating temperature loads, it is evident that the number, width and complexity of fractures are significantly increased after treatment with alternating temperature loads. These differences are primarily reflected in the following aspects:

1) After applying alternating temperature loads, the fracture width on the upper bottom surface is greater than that observed after simple heat treatment. A small amount of fragmented debris detaches from the edges of the prefabricated borehole, while on the upper bottom surface after simple heat treatment, macroscopic fractures are predominantly observed.
2) On the side surface of the rock sample treated with alternating temperature loads, multiple main fractures are formed and numerous branch fractures extend from different positions along these fractures. In contrast, after simple heat treatment, the fracture network structure is relatively simpler.
3) After applying alternating temperature loads, a considerable amount of fragmented debris detaches from the borehole on the lower bottom surface, and numerous microfractures appear around the borehole. In contrast, after simple heat treatment, less fragmented debris detaches from the borehole on the lower bottom surface.

5. Discussion

After being fractured by the high-efficiency expanding agent, the fracture propagation exhibits significant randomness and the surface fracture distributions vary. To better understand the mechanism of fracture propagation during the expansion fracturing process in HDR, this section discusses the expansion-induced fracture network propagation mechanism from three key aspects: the chemical reaction principle of the high-efficiency expanding agent, the rock-breaking mechanical effects, and the expansion fracturing process itself.

5.1 Fracturing principle

5.1.1 Chemical reaction process

The high-efficiency expanding agent used in this study was developed by the China Building Materials Academy in 1982. It is made by mixing special clinker, which is calcined at temperatures above 1,400 °C in a rotary kiln, with a small quantity of additives. The clinker primarily consists of quicklime (CaO) and tricalcium silicate (Ca_3SiO_3), while the additives mainly include magnesium oxide (MgO) and sodium carbonate (Na_2CO_3).

High-efficiency expanding agents are potent and safe materials used for crushing hard substances like marble and gra-

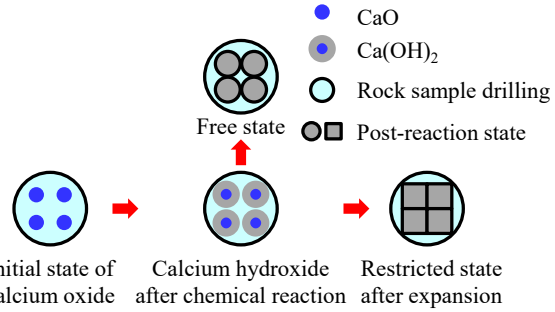

Fig. 11. Simulation of molecular expansion during hydration reaction.

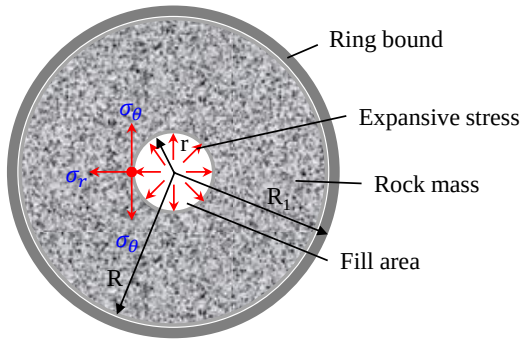

Fig. 12. Diagram of rock failure mechanism by high-efficiency expansion agent.

nite. First, the agent is mixed with water to form a slurry, which is then poured into the rock's boreholes. Within 3 to 24 hours, the crushing process occurs without vibration, noise, or the release of harmful gases. The primary chemical reaction involves calcium oxide reacting with water, as described by the following equation:

$$CaO + H_2O = Ca(OH)_2 \quad (3)$$

This chemical reaction demonstrates that when the high-efficiency expanding agent is mixed with water, it reacts to form calcium hydroxide and releases heat in the process.

5.1.2 Volume expansion process

Taking the chemical reaction equation as a basis, it can be deduced that the product formed by mixing the high-efficiency expanding agent with water is calcium hydroxide. According to relevant sources, the density of calcium hydroxide is 2.24 g/cm^3, that of calcium oxide is 3.35 g/cm^3, and that of water is 1 g/cm^3. Following the principle of mass conservation in chemical reactions, the total mass of the substances involved before and after the reaction remains constant. Therefore, the mass of calcium hydroxide produced equals the combined mass of calcium oxide and water. Since the density of calcium hydroxide is less than the combined density of calcium oxide and water, the volume of the generated calcium hydroxide is greater than that of the reactants, which results in volume expansion during the expansion fracturing process.

Molecular-scale characterization demonstrates increased intermolecular spacing in $Ca(OH)_2$ systems relative to CaO-H_2O complexes. The surface area of the generated calcium hydroxide can reach 10-20 m^2/g, and its volume expands to two to three times the original value. Fig. 11 illustrates the volume models of the high-efficiency expanding agent molecules under various confinement states during the chemical reaction process. In the free state, the products evenly fill the confined volume, with little to no compression between molecules, resulting in no-expansion stress after the chemical reaction. However, as the products undergo volume expansion within the constrained borehole, their molecules come into contact and compress. Then, the stress concentration at the center of the confined space propagates to surrounding areas, generating expansion stress. When this expansion stress exceeds the tensile strength of the rock sample, fractures extend from the prefabricated borehole and connect to each other, leading to the expansion fracturing of the rock sample.

5.2 Fracturing stage

Expansion fracturing technology utilizes chemical agents to generate controlled fractures in rock formations by precise stress manipulation. This method creates radial circumferential stresses by combining internal expansion forces with external confinement, enabling predictable fracture propagation. As shown in Fig. 12, expansion fracturing involves injecting the expanding agent into the prefabricated boreholes of the rock samples. When the high-efficiency expanding agent reacts within the borehole, it undergoes volume expansion. The constraining effect of borehole walls causes the expansion stress to concentrate, transmitting the force around the walls and converting it into radial circumferential stress. Meanwhile, the thick-walled cylinder surrounding the rock sample provides circumferential restraint. As the high-efficiency expanding agent expands outward, the radial circumferential stress from the inside, combined with the restraint stress from the thick-walled cylinder, compresses the specimen. When the stress reaches the peak strength of the HDR, microfractures begin to form within the rock sample and continue to develop. These fractures expand and connect, ultimately forming macroscopic fractures and achieving the expansion fracturing of the HDR.

The expansion fracturing process of HDR samples can be divided into three stages, as presented below.

5.2.1 Micro-fracture propagation stage

When the high-efficiency expanding agent is mixed with water, a chemical reaction occurs, causing the volume of calcium hydroxide to increase. This results in the generation of expansion stress within the confined space of the borehole, acting on its inner walls. At the same time, the thick-walled cylinder surrounding the rock sample applies a reverse restraining force. As the stress concentration builds and exceeds the peak strength of the rock sample, the process progresses through the elastic deformation phase, followed by the plastic deformation phase, before the expansion fracturing occurs.

The stress state of the rock surrounding the inner wall of the borehole can be described using radial stress and circumferential stress in a cylindrical coordinate system. The force generated when the high-efficiency expanding agent undergoes volume expansion is given by the following equation (Lamé

and Clapeyron, 1831):

$$\begin{Bmatrix} \sigma_\theta \\ \sigma_r \end{Bmatrix} = P\frac{R^2}{(R+d)^2-R^2}\left[1 \pm \frac{(R+d)^2}{r^2}\right] \tag{4}$$

where σ_r is the radial stress around the wellbore during the expansion process, while σ_θ is the circumferential stress around the wellbore during the same process. P represents the expansion force acting on the borehole wall, R represents the radius of the borehole, r represents the radius at a certain distance from the borehole wall, and d is the thickness at a certain distance from the inner wall of the borehole.

During the micro-fracture propagation stage, as the chemical reaction of the expanding agent progresses, the expansion stress gradually increases until reaching the peak stress of the rock sample. At this point, micro-fractures begin to form near the wellbore.

5.2.2 Fracture development stage

During the fracture propagation process, micro-fractures progressively coalesce and develop into dominant macroscopic fractures. On the basis of Griffith's fracture mechanics theory, the critical stress intensity factor (K_{IC}) for HDR failure during expansion fracturing can be expressed as (Irwin, 1957):

$$K_{IC} = YP\sqrt{\pi a} \tag{5}$$

where a represents the fracture length, Y represents the fracture shape factor, which depends on the fracture type. To ensure that the fracture continues to expand, the expansion stress must meet the following condition:

$$P \geq \frac{K_{IC}}{Y\sqrt{\pi a}} \tag{6}$$

5.2.3 Rock sample failure stage

As the number of fractures continues to increase, the internal fractures of the rock sample also expand and propagate. Eventually, when these fractures interconnect and form larger macroscopic fractures, expansion fracturing occurs under the sustained action of expansion force. This process leads to the development of a complex fracture network, enabling the effective breakdown of the rock sample.

5.3 Mechanical mechanism

In order to investigate the expansion mechanism of artificial fracture networks on the basis of thermal-mechanical coupling, this study conducted an expansion fracturing experiment of HDR subjected to alternating temperature loads.

In the boreholes of rock samples, the high-efficiency expanding agent reacts with water in a confined space, releasing energy and causing volume expansion. The expanding agent applies expansion force to the borehole wall, while the rock sample exerts an equal and opposite reaction force to maintain its original shape. At the same time, due to the clamping effect of the thick-walled cylinder surrounding the rock sample, circumferential stress is applied to the center of the rock.

As the chemical reaction progresses, the volume expansion rate gradually increases, and the expansion force directed towards the inner borehole wall eventually exceeds the peak strength of the rock. This results in the breaking of mineral particles with relatively low bonding strength, leading to the formation of micro-pores. As the expansion stress increases further, the porosity of the rock sample also rises, and these micro-pores formed connect to form microscopic fractures.

The micro-fractures undergo progressive expansion, propagation and coalescence, ultimately developing into macroscopic fracture networks. These fractures radially propagate through the rock matrix until they intersect the sample boundaries, establishing a continuous fracture plane, marking the completion of the expansion fracturing process. As a consequence of volumetric constraints, the high-efficiency expanding agent within the borehole is subsequently expelled through both the upper and lower borehole sections, thereby finalizing the entire expansion fracturing procedure.

6. Conclusions

This study investigated the expansion characteristics of engineered fracture networks in HDR under thermal cycling conditions, with particular emphasis on the coupled effects of temperature variations and mechanical loading on the fracture propagation dynamics. The applied research methodology incorporates the quantitative analysis of fracture network complexity by fractal dimension characterization and systematic evaluation of post-failure fracture patterns. Furthermore, the rock fracturing mechanism induced by high-efficiency expanding agents was thoroughly examined to elucidate the fundamental processes governing fracture network development. The principal findings can be summarized as follows:

1) The fractal dimension of the expansion fracture network in HDR subjected to alternating temperature loads is notably higher compared to those treated with simple heat treatment. This is directly correlated with temperature, showing a 3.86% rise at 500 °C. The analysis of fractal dimensions across the upper and lower bottom surfaces, as well as the side surface of the rock samples, reveals that the fracture networks after alternating temperature loads exhibit higher fractal dimensions than those after simple heat treatment. The most significant increases in fractal dimension occur between 500 and 600 °C, with the upper bottom surface, lower bottom surface, and side surface showing increases of 7.4%, 7.8% and 6.5%, respectively.
2) The number and complexity of expansion fracture networks in HDR subjected to alternating temperature loads are greater than those observed after simple heat treatment. The fracture morphologies on the upper and lower bottom surfaces, as well as the side surface of the rock samples, reveal that after alternating temperature loads, fractures on the upper bottom surface, predominantly form a double-wing symmetrical structure. At 600 °C, both the number of branch fractures and the fracture width significantly increase, while a considerable amount of fragmented debris collapses near the borehole. On the side surface, multiple branch fractures extend outward from the main fracture after expansion fracturing. These

observations indicate that alternating temperature loads significantly enhance the complexity of the expansion fracture network in HDR.

3) When mixed with water, the high-efficiency expanding agent undergoes a chemical reaction that produces calcium hydroxide while also expanding in volume and releasing heat. This reaction rapidly increases the expansion stress near the borehole wall within the confined space. As the expansion stress surpasses the peak strength of rock sample, numerous microfractures form, gradually expanding and connecting to create macroscopic fractures. This sequence of events leads to the successful expansion fracturing of the HDR.
4) Overall, this work provides new insights are provided into hydraulic fracturing in deep geothermal reservoirs. By increasing the complexity of induced fracture network, researchers can unlock the full potential of EGS and establish it as a reliable and sustainable source of clean energy.

Acknowledgements

This research was financially supported by the National Natural Science Foundation Project (Nos. 52474001 and 52274002), and the PetroChina Science and Technology Innovation Foundation Project (No. 2021DQ02-0201).

Conflict of interest

The authors declare no competing interest.

References

Barton, C. C. Fractal analysis of scaling and spatial clustering of fractures, in Fractals in the Earth Sciences, edited by Barton, C. C., La Pointe, P. R., Springer, Boston, pp. 141-178, 1995.

Cai, J., Wei, W., Hu, X., et al. Fractal characterization of dynamic fracture network extension in porous media. Fractals, 2017, 25(2): 1750023.

Cheng, Y., Zhang, Y., Yu, Z., et al. An investigation on hydraulic fracturing characteristics in granite geothermal reservoir. Engineering Fracture Mechanics, 2020, 237: 107252.

Cheng, Y., Zhang, Y., Yu, Z., et al. Experimental and numerical studies on hydraulic fracturing characteristics with different injection flow rates in granite geothermal reservoir. Energy Science & Engineering, 2021, 9(1): 142-168.

Deng, S., Xiong, F., Liu, Y., et al. Temperature-dependent permeability model of granite after thermal treatment based on energy dissipation theory and fractal theory. Rock Mechanics and Rock Engineering, 2023, 56(9): 6321-6335.

Dong, Y., Wang, D., Qin, H., et al. Device for simulating fracture morphology of hot dry rock. CN202021009205.3, 2021.

Guo, T., Tang, S., Liu, S., et al. Numerical simulation of hydraulic fracturing of hot dry rock under thermal stress. Engineering Fracture Mechanics, 2020, 240: 107350.

Guo, T., Zhang, S., Ge, H. A new method for evaluating ability of forming fracture network in shale reservoir. Rock and Soil Mechanics, 2013, 34(4): 947-954. (in Chinese)

Hou, B., Chen, M., Li, Z., et al. Propagation area evaluation of hydraulic fracture networks in shale gas reservoirs. Petroleum Exploration and Development, 2014, 41(6): 833-838.

Irwin, G. R. Analysis of stresses and strains near the end of a crack traversing a plate. Journal of Applied Mechanics, 1957, 24(3): 361-364.

Kao, J., Jin, Y., Fu, W., et al. Experimental research on the morphology of hydraulic fractures in deep shale under high difference of *in-situ* horizontal stresses. Chinese Journal of Rock Mechanics and Engineering, 2018, 37(6): 1332-1339. (in Chinese)

Kumari, W. G. P., Ranjith, P. G., Perera, M. S. A., et al. Hydraulic fracturing under high temperature and pressure conditions with micro CT applications: Geothermal energy from hot dry rocks. Fuel, 2018, 230: 138-154.

Lamé, G., Clapeyron, B. Mémoire sur l'équilibre intérieur des corps solides homogènes. Journal für die reine und angewandte Mathematik, 2009, 1831(7): 381-413. (in French)

Li, C., Tu, J., Xie, H., et al. Tensile behavior and damage mechanisms of hot dry rock under thermal shock fatigue and seawater dissolution. Advances in Geo-Energy Research, 2024, 13(2): 132-145.

Liu, Y., Zhang, F., Weng, D., et al. Two-phase flow thermo-hydro-mechanical modeling for a water flooding field case. Rock Mechanics Bulletin, 2024, 3(3): 100125.

Li, Y. Simulation of the interactions between multiple hydraulic fractures and natural fracture network based on discrete element method numerical modeling. Energy Science & Engineering, 2020, 8(8): 2922-2937.

Li, Y., Hu, W., Zhang, Z., et al. Numerical simulation of hydraulic fracturing process in a naturally fractured reservoir based on a discrete fracture network model. Journal of Structural Geology, 2021, 147: 104331.

Luo, T., Liu, Y. Effects of thermal stress in hot dry rock fracturing. SPE Drilling & Completion, 2022, 37(4): 353-363.

Mandelbrot, B. How long is the coast of Britain? Statistical self-similarity and fractional dimension. Science, 1967, 156(3775): 636-638.

Ma, W., Yang, C., Ahmed, S. F., et al. Effects of thermophysical parameters of fracturing fluid on hot dry rock damage in hydraulic fracturing. Geomechanics for Energy and the Environment, 2022, 32: 100405.

Moska, R., Labus, K., Kasza, P. Hydraulic fracturing in enhanced geothermal systems-field, tectonic and rock mechanics conditions-A review. Energies, 2021, 14(18): 5725.

Moska, R., Labus, K., Kasza, P. Dynamic elastic properties, petrophysical parameters and brittleness of hot dry rocks

from prospective areas of central europe. Advances in Geo-Energy Research, 2024, 14(2): 90-105.

Pan, J., Zhang, L., Ma, Y., et al. Effect of thermal cracking on the tensile strength of granite: Novel insights into numerical simulation and fractal dimension. Fractal and Fractional, 2024, 8(11): 669.

Sheng, G., Su, Y., Wang, W. A new fractal approach for describing induced-fracture porosity/permeability/compressibility in stimulated unconventional reservoirs. Journal of Petroleum Science and Engineering, 2019, 179: 855-866.

Wang, D., Dong, Y., Li, Y., et al. Numerical simulation of heat recovery potential of hot dry rock under alternate temperature loading. Unconventional Resources, 2022, 2: 170-182.

Wang, D., Dong, Y., Wang, Q., et al. Experimental study on the evolution of mechanical properties of hot dry rocks under alternating temperature loads. Geothermics, 2023a, 107: 102599.

Wang, D., Zhu, H., Micheal, M., et al. Coupled heat-fluid-solid numerical study on heat extraction potential of hot dry rocks based on discrete fracture network model. Energy Geoscience, 2023b, 4(4): 100159.

Wang, H. Hydraulic fracture propagation in naturally fractured reservoirs: Complex fracture or fracture networks. Journal of Natural Gas Science and Engineering, 2019, 68: 102911.

Wang, Q., Wang, D., Fu, W., et al. Effects of saturated fluids on petrophysical properties of hot dry rock at high temperatures: An experimental study. Geothermics, 2024a, 121: 103048.

Wang, Q., Wang, D., Yu, B., et al. Evolution of elastic-plastic characteristics of rocks within middle-deep geothermal reservoirs under high temperature. Natural Resources Research, 2024b, 33(4): 1573-1596.

Wang, S., Zhou, J., Zhang, L., et al. Numerical insight into hydraulic fracture propagation in hot dry rock with complex natural fracture networks via fluid-solid coupling grain-based modeling. Energy, 2024c, 295: 131060.

Xue, Y., Liu, S., Chai, J., et al. Effect of water-cooling shock on fracture initiation and morphology of high-temperature granite: Application of hydraulic fracturing to enhanced geothermal systems. Applied Energy, 2023, 337: 120858.

Yang, Z., Tao, M., Ranjith, P. G., et al. Multiscale damage and thermal-stress evolution characteristics of rocks with thermal storage potential under thermal shocks. Journal of Energy Storage, 2024, 83: 110631.

Yu, J., Li, N., Hui, B., et al. Experimental simulation of fracture propagation and extension in hydraulic fracturing: A state-of-the-art review. Fuel, 2024, 363: 131021.

Zhang, Z., Fu, X., Yuan, W., et al. The influence of the fractal dimension on the mechanical behaviors of the soil-rock mixture: A case study from southwest china. Fractal and Fractional, 2023, 7(2): 106.

Zheng, P., Xia, Y., Yao, T., et al. Formation mechanisms of hydraulic fracture network based on fracture interaction. Energy, 2022, 243: 123057.

Zhuang, D., Yin, T., Fu, Q., et al. Fractal fracture toughness measurements of heat-treated granite using hydraulic fracturing under different injection flow rates. Theoretical and Applied Fracture Mechanics, 2022, 119: 103340.